Vibration Analysis of a Cracked Rotor with an Unbalance Influenced Breathing Mechanism

Joseph P. Spagnol, Helen Wu, and Chunhui Yang
School of Computing, Engineering and Mathematics, Western Sydney University, Penrith, Australia
Email: {j.spagnol, helen.wu, r.yang}@westernsydney.edu.au

***Abstract*—The breathing mechanism of a shaft crack is an advantageous tool for describing the stiffness changes that occur in the shaft. Unbalance can affect the breathing mechanism of the crack and may produce behaviors that are significantly different to weight-dominant breathing patterns. As such, cracked rotors with large permissible residual unbalance will require new models to accurately describe the vibration of the rotor. In this study, the breathing mechanism of a crack is modeled to include the effects of unbalance loading and then the time-varying stiffness of the cracked rotor is determined. Consequently, MATLAB ode15s function (an adaptive step solver) is used to numerically integrate the equations of motion of a finite element cracked rotor that incorporates the proposed crack breathing model. The predicted 1X, 2X and 3X harmonic components of a rotor with deep crack (80% of radius) were seen to significantly differ between the proposed model and an existing weight-dominant model. Due to the significant differences in the breathing mechanisms and vibration results of the two models, the weight-dominant breathing model was deemed unsuitable for modeling the vibration of cracked rotors with large permissible residual unbalance.**

***Index Terms*—cracked rotor, crack breathing, fatigue crack, unbalanced rotor, vibration of cracked rotor**

I. Introduction

Producing accurate numerical models of fatigue cracks are a preliminary, albeit important, tool for safeguarding rotating machinery from fatigue failure. Numerical models aim to predict vibration behavior in cracked rotors so to identify cracks in real rotors before they become a detriment to the machine. The presence of superharmonics (mostly 2X and 3X) in the frequency spectrum of a rotor has been shown to indicate the presence of fatigue cracks. Unfortunately, other rotor faults such as shaft bowing, misalignment and rotor impact-rubbing may also result in the presence of superharmonics.

Many studies assume that dynamic loading has a negligible effect on the behavior of a crack. Models that adhere to this assumption are typically known as 'weight-dominant' models and are generally accepted as being accurate for large turbogenerators. However, several studies show that weight-dominance is not suitable for lightweight rotors, vertical-axis rotors or rotors operating around their critical speed [1] and [2]. Rubio et al. [3] studied the effect of unbalance on the crack breathing behavior in a numerical simulation using Abaqus. In [4], the crack breathing mechanism is modeled by calculating Stress Intensity Factor (SIF) of the fatigue crack. For each iteration, the updated rotor displacements are used to recalculate the forces acting on the crack and SIF. The authors of [4] reported that at speeds sufficiently lower or higher than critical speed the crack breathes normally. However, as the accelerating rotor approached critical speed the crack no longer breathed normally and at times fully closing for a short duration after passing the critical speed. Bachschmid et al. [1] suggest the breathing mechanism of the shaft is not only governed by the shaft rotation angle but also by vibration dependent inertia forces. It was found that during unstable vibration the crack is almost always open, however the unbalance angle may cause the crack to close more and therefore avoid instability. Also, the vibration amplitudes of the cracked turbogenerator demonstrated significance in the 2X harmonic component not only around one-half of the critical speed, but also after the critical speed. Cheng et al. [2] introduced a crack breathing model that dynamically modifies the elastic force acting on the crack by considering the whirling of the shaft and the position of the crack relative to the bending direction. The authors discovered that the crack may breathe weakly twice during one revolution when weight-dominance is not assumed. El Arem and Nguyen [5] also describe the breathing mechanism with reliance on the vibration response of the system. Their cracked rotor model demonstrates flexibility through the ability to examine the weight-dominant condition.

This study investigates the suitability of a weight-dominant breathing mechanism for predicting the vibration behavior of a cracked rotor with large permissible residual unbalance. In Section II, an alternative breathing model is formulated. The proposed breathing model is applied to the rotor outlined in Section III and its vibration behavior is examined in Section IV.

II. Crack Breathing Model

A. Unbalance Influenced Breathing Mechanism

In heavy, rigid horizontal rotors, such as large turbogenerators, the bending moments due to dynamic forces are considered to be negligible relative to static bending moments. In these rotors, the crack breathing

Manuscript received August 10, 2017; revised December 4, 2017.

doi: 10.18178/ijmerr.7.1.22-29

mechanism is common described as being governed by the weight of the rotor only (weight-dominant models). However, in rotors with higher specific residual unbalance tolerances this assumption is not appropriate.

The model in Fig. 1 aims to describe the breathing response of a singular transverse crack in a horizontal rotor without the assumption of weight-dominance. The premise of crack breathing is the same whether or not the rotor is considered to be weight-dominant. The gradual opening and closing of a fatigue crack (represented by the shaded minor segment of the cracked shaft cross-section) is dependent on the proximity of the crack direction relative to the direction of the bending load. Weight-dominant models assume that the weight of the rotor (mg) is a sole contributor to the breathing behavior of a crack, therefore in these models the bending load always acts in the direction of the negative Y-axis. Also, the relative direction between the bending load and the crack is described by the angle of rotation of the shaft only. When rotating unbalance F_{me} (numerically equal to the eccentricity multiplied by the square of the rotor speed) is introduced into the rotor system, the bending load P is calculated as the vector sum in the X and Y directions of the unbalance and weight force components, as seen in (1) and (2),

$$P_X = F_{me}\sin(\Omega t + \beta) \tag{1}$$

$$P_Y = F_{me}\cos(\Omega t + \beta) + mg\,. \tag{2}$$

where Ωt is the direction of the crack (Ωt = 0 when crack direction is at the negative Y-axis) and the angle β is the direction of the unbalance force relative to the crack direction. The unbalance force F_{me} is assumed to act in the radial direction at an angle of δ from the negative Y-axis, where δ is calculated by (3)

$$\delta = \tan^{-1}\left[\frac{\sin(\Omega t + \beta)}{\cos(\Omega t + \beta) + \eta}\right]. \tag{3}$$

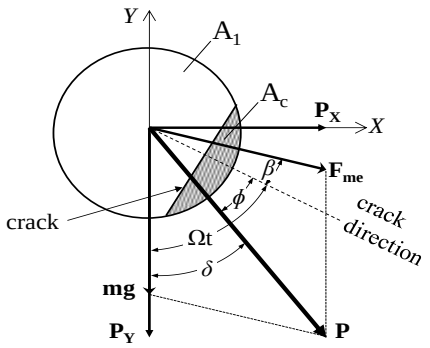

Figure 1. Force diagram and chordal representation of a cracked rotor.

The parameter η is equal to $mg/m_{ed}\Omega^2$ i.e. the ratio of the weight force to unbalance force, where m_{ed} is the unbalance eccentricity in kg·m, Ω is the rotor speed, g is the gravitational acceleration constant and m is the total mass of the rotor. The proximity of the bending load P to the crack direction (dubbed effectual loading angle ϕ in this paper) can then be calculated by (4). Modification to the co-domain of δ and ϕ is performed to return values between 0 and 2π radians.

$$\phi = \Omega t - \delta\,. \tag{4}$$

B. Area Moment of Inertia of Rotating Cracked Cross-Section

The authors in [6] demonstrate that change in stiffness of a rotating shaft due to a transverse crack can be modeled by a reduction of the area moment of inertia of the shaft cross-section. As such, a number of studies [7] and [8] develop models that calculate the time-varying area moments of inertia of the cracked shaft cross-section. In these existing studies on cracked rotors the area moments of inertia values are calculated based on weight-dominant crack breathing models so the change in area moment of inertia is not influenced by rotating unbalance.

The effectual loading angle from (4) can be used to modify existing weight-dominant area moment of inertia models. The basis for modifying the existing model is depicted through the geometric similarity seen in Fig. 2. At any instant, the non-cracked area can be determined by the sum of areas A_1 and A_2. When ϕ = Ωt, the geometry of the two models is equivalent, in particular the area moment of inertia of the non-cracked area about the unbalanced rotor's $\overline{X'}$ and $\overline{Y'}$ axes is equivalent to the weight-dominant rotor's $\overline{X}$ and $\overline{Y}$ axes, respectively.

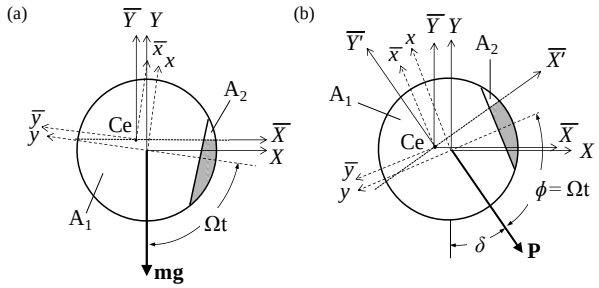

Figure 2. Breathing model of cracked shaft systems showing identical cracked and non-cracked areas between the (a) weight-dominant rotor and (b) unbalanced rotor.

As such, the time-varying area moments of inertia in this study are obtained by modifying the method seen in [8]. Their procedure is as follows: the area moments of inertia of the non-cracked area A_1 about the rotating *x* and *y* axes as seen in Fig. 2(a) are given by

$$I_1 = I - I_X^c \tag{5}$$

$$I_2 = I - I_Y^c \tag{6}$$

where $I = \pi R^4/4$ is the area moment of inertia of the full circular cross-section of the shaft, I_X^c and I_Y^c are the area moments of inertia of the crack segment about the rotating x and y axes, respectively. The values of I_X^c and I_Y^c are calculated by

$$I_X^c = \frac{\pi R^4}{8} - \frac{R^4}{4}\left[(1-\mu)(2\mu^2 - 4\mu + 1)\gamma + \sin^{-1}(1-\mu)\right] \tag{7}$$

$$I_Y^c = \frac{R^4}{12}\left[(1-\mu)(2\mu^2-4\mu-3)\gamma + 3\sin^{-1}(\gamma)\right]. \quad (8)$$

The area moments of inertia of the non-cracked area about the rotating centroidal axes, $\bar{x}$ and $\bar{y}$ can then be calculated by

$$\bar{I}_1 = I_1 - A_1 e^2 \quad (9)$$

$$\bar{I}_2 = I_2 . \quad (10)$$

The time-varying area moments of inertia of the total non-cracked area about the weight-dominant rotor centroid axes, can be approximated by

$$\hat{I}_{\bar{X}}(t) = I - (I - \bar{I}_1) f_1(t) \quad (11)$$

$$\hat{I}_{\bar{Y}}(t) = I + (I - \bar{I}_1) f_1(t) - (2I - \bar{I}_1 - \bar{I}_2) f_2(t) \quad (12)$$

where $f_1(t)$ and $f_2(t)$ are the breathing functions and are defined as

$$f_1(t) = \frac{1}{2^m}\left[\binom{m}{m/2} + 2\sum_{j=0}^{(m/2)-1}\binom{m}{j}\cos\left((m-2j)\frac{\Omega t}{2}\right)\right] \quad (13)$$

$$f_2(t) = \frac{1}{2^m}\left[-\frac{\theta_1+\theta_2}{2} + \frac{2}{(\theta_2-\theta_1)}\times \sum_{i=1}^{p}\frac{\cos(i\theta_2)-\cos(i\theta_1)}{i^2}\cos(i\Omega t)\right] \quad (14)$$

The terms p and m are positive even integers that control the curvature and shape of the breathing functions. Readers should consult the original source for the calculation of θ_1 and θ_2. Again, due to the geometric equivalence between the weight-dominant rotor and the unbalanced rotor, the Ωt term in (13) and (14) can be replaced by the effectual loading angle ϕ. In doing so, the area moment of inertia of the total non-cracked area about the unbalanced shaft's $\bar{X}'$ and $\bar{Y}'$ axes is obtained. From [9] the product of inertia of the total non-cracked area can be approximated by

$$\hat{I}_{\bar{X}\bar{Y}}(t) = -\left(\frac{I_1 - I_2}{2} + \frac{A_1 e^2}{2}\right)\times \sum_{k=1}^{p}\frac{2\bar{\theta}_2\sin(\pi - k\bar{\theta}_2)}{\pi^2 - k^2\bar{\theta}_2^2}\sin(k\Omega t) \quad (15)$$

where $\bar{\theta}_2 = 0.8\times\theta_2$. The Ωt term is replaced by ϕ to calculate the product of inertia of the non-cracked area about the unbalance rotor's $\bar{X}'$ and $\bar{Y}'$ axes. Consequently, (16) to (18) are used to obtain the unbalanced rotor's area moment of inertia of the non-cracked area about the desired $\bar{X}$ and $\bar{Y}$ axes.

$$I_{\bar{X}}(t,\delta) = \frac{\hat{I}_{\bar{X}}(t)+\hat{I}_{\bar{Y}}(t)}{2} + \frac{\hat{I}_{\bar{X}}(t)-\hat{I}_{\bar{Y}}(t)}{2}\cos(2\delta) + \hat{I}_{\bar{X}\bar{Y}}(t)\sin(2\delta) \quad (16)$$

$$I_{\bar{Y}}(t,\delta) = \frac{\hat{I}_{\bar{X}}(t)+\hat{I}_{\bar{Y}}(t)}{2} - \frac{\hat{I}_{\bar{X}}(t)-\hat{I}_{\bar{Y}}(t)}{2}\cos(2\delta) - \hat{I}_{\bar{X}\bar{Y}}(t)\sin(2\delta) \quad (17)$$

$$I_{\bar{X}\bar{Y}}(t,\delta) = -\frac{\hat{I}_{\bar{X}}(t)-\hat{I}_{\bar{Y}}(t)}{2}\sin(2\delta) + \hat{I}_{\bar{X}\bar{Y}}(t)\cos(2\delta) \quad (18)$$

C. Element Stiffness Matrix of Breathing Crack

As the crack breathes, the alignment of the principal centroidal axes changes. Fundamental shaft element stiffness matrices in literature are only applicable to the principal centroidal axes of the cracked shaft. Further modification of existing element stiffness matrices is required so that the matrices are written in terms of the $\bar{X}$ and $\bar{Y}$ axes.

A non-closed crack results in an irregular non-cracked cross-section (shaded section in Fig. 3) with principal centroidal axes W and V at some angle α from the centroidal axes $\bar{X}$ and $\bar{Y}$ as seen in Fig. 3. In order to obtain the stiffness matrix of the non-cracked area in terms of the $\bar{X}$ and $\bar{Y}$ axes, the area moments of inertia about the principal centroidal axes must be calculated first then used to obtain the area moments of inertia about the $\bar{X}$ and $\bar{Y}$ axes.

The instantaneous area moment of inertia values about the principal centroidal directions, I_W and I_V, are calculated using Mohr's circle for area moments of inertia, as in (19) and (20).

$$I_W = \frac{I_{\bar{X}}+I_{\bar{Y}}}{2} + \sqrt{\left(\frac{I_{\bar{X}}-I_{\bar{Y}}}{2}\right)^2 + I_{\bar{X}\bar{Y}}{}^2} \quad (19)$$

$$I_V = \frac{I_{\bar{X}}+I_{\bar{Y}}}{2} - \sqrt{\left(\frac{I_{\bar{X}}-I_{\bar{Y}}}{2}\right)^2 + I_{\bar{X}\bar{Y}}{}^2} \quad (20)$$

The values $I_{\bar{X}}$, $I_{\bar{Y}}$ and $I_{\bar{X}\bar{Y}}$ are obtained from (16) to (18). From [10], the element stiffness matrix $[k_p]$ of a beam element with an irregular cross-section is given as

$$[k_p] = \frac{E}{l^3}\begin{bmatrix} 12I_W & 0 & 0 & 6lI_W \\ 0 & 12I_V & -6lI_V & 0 \\ 0 & -6lI_V & 4l^2I_V & 0 \\ 6lI_W & 0 & 0 & 4l^2I_W \\ -12I_W & 0 & 0 & -6lI_W \\ 0 & -12I_V & 6lI_V & 0 \\ 0 & -6lI_V & 2l^2I_V & 0 \\ 6lI_W & 0 & 0 & 2l^2I_W \end{bmatrix} \quad (21)$$

$$\begin{bmatrix} -12I_W & 0 & 0 & 6lI_W \\ 0 & -12I_V & -6lI_V & 0 \\ 0 & 6lI_V & 2l^2I_V & 0 \\ -6lI_W & 0 & 0 & 2l^2I_W \\ 12I_W & 0 & 0 & -6lI_W \\ 0 & 12I_V & 6lI_V & 0 \\ 0 & 6lI_V & 4l^2I_V & 0 \\ -6lI_W & 0 & 0 & 4l^2I_W \end{bmatrix}$$

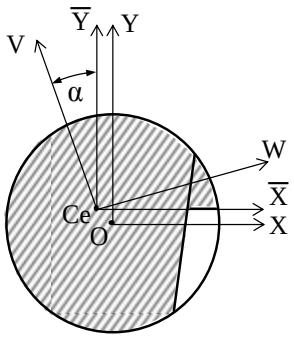

Figure 3. Irregular cross-section of a cracked shaft with a partially open crack showing the principal axes of the cracked cross-section.

The element stiffness matrix from the principal centroidal axes in (21) can be transformed to the $\bar{X}$ and $\bar{Y}$ using the transformation matrix T [10] in Eq. (22), where α is calculated by Mohr's circle for area moment of inertia. The values for α are summarized in Table I. It should be noted that $\psi = \tan^{-1}\left[2I_{\bar{X}\bar{Y}} / \left(I_{\bar{Y}} - I_{\bar{X}}\right)\right]$.

$$[T] = \begin{bmatrix} \cos(\alpha) & -\sin(\alpha) & 0 & 0 \\ \sin(\alpha) & \cos(\alpha) & 0 & 0 \\ 0 & 0 & \cos(\alpha) & -\sin(\alpha) \\ 0 & 0 & \sin(\alpha) & \cos(\alpha) \\ 0 & 0 & 0 & 0 \\ 0 & 0 & 0 & 0 \\ 0 & 0 & 0 & 0 \\ 0 & 0 & 0 & 0 \end{bmatrix} \quad (22)$$

$$\begin{bmatrix} 0 & 0 & 0 & 0 \\ 0 & 0 & 0 & 0 \\ 0 & 0 & 0 & 0 \\ 0 & 0 & 0 & 0 \\ \cos(\alpha) & -\sin(\alpha) & 0 & 0 \\ \sin(\alpha) & \cos(\alpha) & 0 & 0 \\ 0 & 0 & \cos(\alpha) & -\sin(\alpha) \\ 0 & 0 & \sin(\alpha) & \cos(\alpha) \end{bmatrix}.$$

The modified instantaneous cracked element stiffness about the $\bar{X}$ and $\bar{Y}$ axes is then calculated by

$$[k_{ce}] = [T][k_p][T]^T \quad (23)$$

It is important to note that the use of the area moments of inertia values from (16) to (18) in the proposed stiffness matrix are applicable whether a weight-dominant or unbalance approach is intended. A value of $\eta = \infty$ should be used if a weight-dominant approach is intended. Also, (16) to (18) are applicable to all crack states, therefore following the procedure in this sub-section will obtain the elemental stiffness matrix at every instance of the breathing crack.

TABLE I. VALUE OF α REQUIRED FOR TRANSFORMATION MATRIX

Value of α	Condition 1	Condition 2
ψ/2	$I_{\bar{X}\bar{Y}} \neq 0$	$I_{\bar{X}} > I_{\bar{Y}}$
-π/2 + ψ/2	$I_{\bar{X}\bar{Y}} < 0$	$I_{\bar{X}} < I_{\bar{Y}}$
0	$I_{\bar{X}\bar{Y}} = 0$	$I_{\bar{X}} \geq I_{\bar{Y}}$
π/2	$I_{\bar{X}\bar{Y}} = 0$	$I_{\bar{X}} < I_{\bar{Y}}$
π/4	$I_{\bar{X}\bar{Y}} > 0$	$I_{\bar{X}} = I_{\bar{Y}}$
π/2 + ψ/2	$I_{\bar{X}\bar{Y}} > 0$	$I_{\bar{X}} < I_{\bar{Y}}$
-π/4	$I_{\bar{X}\bar{Y}} < 0$	$I_{\bar{X}} = I_{\bar{Y}}$

III. ROTOR MODEL

The finite element rotor model discretized into eight Euler-Bernoulli beam elements (N = 8) seen in Fig. 4 is used in this study. Physically, the rotor model is composed of a flexible shaft with a disk at node 5 and roller-element bearings at each end. The fifth element is the cracked element.

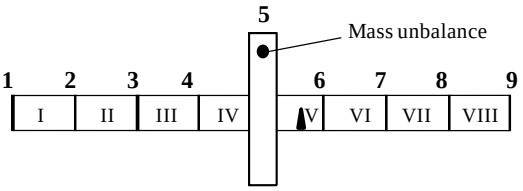

Figure 4. Finite element model of cracked rotor with disk at mid-span.

The physical specifications of the rotor model are based on the SpectraQuest MFS-RDS (as summarized in Table II). Symmetric roller-element bearings with stiffness values $k_{xx} = k_{vv} = 7 \times 10^5$ and damping values $c_{xx} = c_{yy} = 2 \times 10^3$ are also used.

TABLE II. PHYSICAL SPECIFICATIONS OF ROTOR MODEL

Parameter	Disk	Shaft
Material density (kg/m^3)	2700	7800
Elastic modulus (Pa)	2.1×10^{11}	2.1×10^{11}
Thickness or length (m)	0.0122	0.724
Outer radius (m)	0.0762	0.0158
Inner radius (m)	0.0158	0

The equations of motion associated with the cracked rotor system can be described in state-space form as a system of first order differential equations

$$\{\dot{Q}\} = [A]\{Q\} + [B]\{F\} \quad (24)$$

where the state variable, Q, is the $8(N+1) \times 1$ vector of nodal displacements and nodal velocities. The variable F is the vector of loads comprising of rotating unbalance of

the disk and the rotor weight. The matrices [A] and [B] are given by

$$[A]=\begin{bmatrix}[Z] & [I]\\ -[M]^{-1}[K] & -[M]^{-1}[G]\end{bmatrix} \quad (25)$$

$$[B]=\begin{bmatrix}[Z]\\ [M]^{-1}\end{bmatrix} \quad (26)$$

where the matrix [Z] is a 4(N+1)×4(N+1) matrix of zeros and [I] is the 4(N+1)×4(N+1) identity matrix. The global mass, damping/gyroscopic and stiffness matrices of the crack rotor system, [M], [G] and [K], respectively, are 4(N+1)×4(N+1) matrices that can be assembled using standard finite element modeling procedures [11]. The local stiffness matrix of element 5 must be replaced by the cracked element stiffness matrix obtained through (23) so to include the effects of the crack on the rotor. Writing (24) in state-space form allows for direct solution of the equations of motion using MATLAB.

IV. Results and Discussion

The dynamic response of the rotor was obtained using the MATLAB ode15s function, which is an adaptive step solver for stiff problems. Because ode15s is a variable step-solver, the time-steps automatically change throughout the solution depending on the whether the state is changing slowly or rapidly. The generated time increments are typically within the range of 10^{-5} to 10^{-9} seconds. During the simulation the instantaneous stiffness (given by (23)) and instantaneous vector of loads are calculated at each time step so that the final solution accounts for the breathing of the crack and rotating unbalance. When the Discrete Fourier Transforms (DFTs) of the time signals are required regular time steps can be specified for the ode15s function. The simulation still uses a variable step size but the nodal displacements and velocities are particularly presented at the specified time steps.

Fig. 5 examines the change in transverse amplitude during a run-down of a cracked rotor (μ = 0.8) using the proposed breathing model and the weight-dominant breathing model. The transverse amplitude was determined by finding the maximum radial displacement of the disk (node 5) at each rotor speed. Changing the magnitude and angle of the residual unbalance causes the rotor to display different run-down curves, but more importantly, the two models diverge with increased unbalance magnitude. An unbalance magnitude of 10^{-4} kg·m, as in Fig. 5(b), results in a minor difference in the two models. This idea can be demonstrated through (3), where a decrease in m_{ed} results in the bending load behaving more like a static weight load, thus the breathing mechanism behaves like a weight- dominant one. The presence of sub-critical peaks becomes more obvious with decreased unbalance magnitude. These sub-critical peaks (most clearly seen at one-half and one-third of the critical speed) are well known symptoms of cracked rotors and are very commonly seen in cracked rotor literature. The sub-critical peaks appear to be virtually non-existent with larger unbalance magnitude due to the rotating unbalance force dominating the crack breathing mechanism.

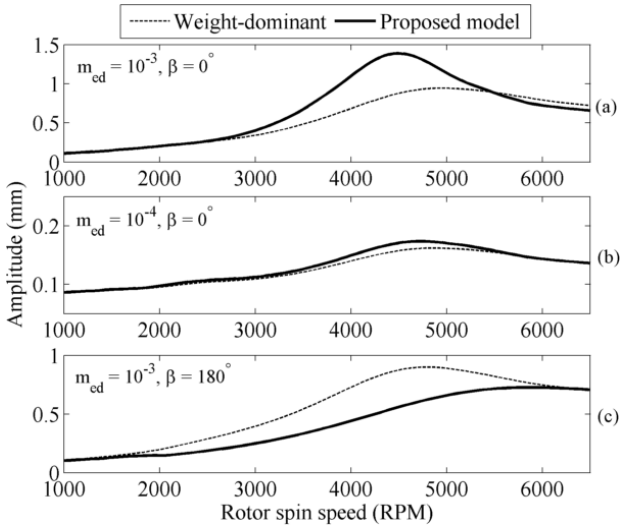

Figure 5. Transverse amplitude during run-down of a cracked rotor (μ = 0.8) with unbalance parameters of (a) $m_{ed} = 10^{-3}$ kg·m, β = 0 °, (b) $m_{ed} = 10^{-4}$ kg·m, β = 0 °and (c) $m_{ed} = 10^{-3}$ kg·m, β = 180 °.

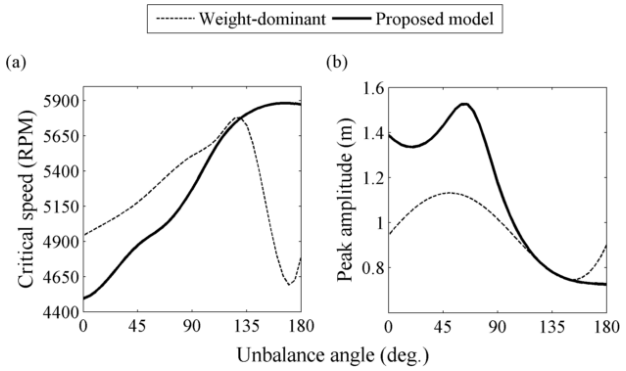

Figure 6. Change in (a) critical speed and (b) peak amplitude of cracked rotor (μ = 0.8) due to a change in unbalance angle. $m_{ed} = 10^{-3}$ kg·m.

Increasing the unbalance magnitude to 10^{-3} kg·m (Fig. 5(a) and (c)) results in significant difference in peak amplitude and critical speed between the two models. This result supports [1] and [2] in suggesting that weight-dominant breathing models are not accurate around the critical speed of cracked rotors. Furthermore, changing the unbalance angle from 0 ° to 180 ° resulted in the proposed model initially having a larger resonant peak at a lower rotor speed to having a smaller resonant peak at a higher rotor speed relative to the weight-dominant model. This phenomenon is further examined through Fig. 6.

In Fig. 6, it is clear that the two models demonstrate a vastly different variation in critical speed and resonant peak amplitude in response to changing the unbalance angle position. For the weight-dominant model, the critical speed sharply rises with an increase in unbalance angle until approximately 135 °and then begins to plateau. The critical speed plateau can be explained by the tendency of the crack to remain closed or mostly closed throughout its rotation when the unbalance mass is placed

about 180° from the crack. Additionally, the peak amplitude of the weight-dominant model appears to change in a sinusoidal manner with an increase in unbalance angle, whereas the proposed model does not.

Examination of the synchronous (1X) and supersynchronous (2X and 3X) harmonic components of the left bearing vibration is an effective tool for detecting cracks in rotors. Fig. 7 and Fig. 8 compare the change in the 1X, 2X and 3X vertical harmonic vibration components obtained during a run-down of the rotor for both the weight-dominant and proposed models. For Fig. 7, a residual unbalance value of 8×10^{-5} kg·m demonstrates a similar change in the harmonic components of both models. Once again, this similarity is expected as the two crack breathing models converge with a decrease in unbalance magnitude. It should be noted that Fig. 7 highlights a typical change in the harmonic components of a cracked rotor: the 1X component is largest at the critical speed, the 2X component is largest at one-half of the critical speed and the 3X component is largest at one-third of the critical speed. In Fig. 8, the residual unbalance is increased to 1×10^{-3} kg·m and two models demonstrate a significant difference in the predicted changes of the 1X, 2X and 3X harmonic components. Cross-examining Fig. 8(a) with Fig. 5(a) shows that the 1X components are largest at the predicted critical speeds (4941 RPM and 4494 RPM for the weight-dominant and proposed models, respectively). Interestingly, the 2X harmonic component peaks at approximately one-half the critical speed for the proposed model however the weight-dominant model does not. It appears that due to the large unbalance mass the 2X harmonic component peaks at approximately 4500 RPM for the weight-dominant model. Fig. 9 shows the predicted breathing response of the proposed and weight-dominant models at 4500 RPM (75 Hz) to provide more insight into the transient change in 2X component. The proposed model predicts that placing the large residual unbalance (1×10^{-3} kg·m) at the same location as the crack ($\beta = 0°$) keeps the crack open (this behavior is also seen in [1] and [3]). On the other hand, the weight-dominant model predicts the crack to breathe normally (gradually open and close) since the breathing mechanism is unaffected by rotating unbalance. As such, prominent 2X and 3X components for the weight-dominant model are to be expected, numerically. Since the weight-dominant model predicts the crack to continue breathing and instead not remain fully open, the weight-dominant model appears to not accurately predict the harmonic components in rotors with large permissible residual unbalance.

Fig. 10 shows a notable difference in trajectory and power spectra of the left bearing between the two models at 4500 RPM. The elliptical trajectory seen for the proposed model is typical for vibration with insignificant 2X and 3X components. The corollary to this is that the introduction of significant 2X and 3X components deviates the orbital trajectory from a circle or ellipse to more intricate shapes. The proposed model's trajectory is larger due to a more significant 1X component at 4500 RPM.

With these findings it is clear that a weight-dominant breathing mechanism is unsuitable for rotors with large permissible residual unbalance. If numerical models fail to correctly estimate the vibration behavior of these rotors then the models are ineffective as tools for crack detection.

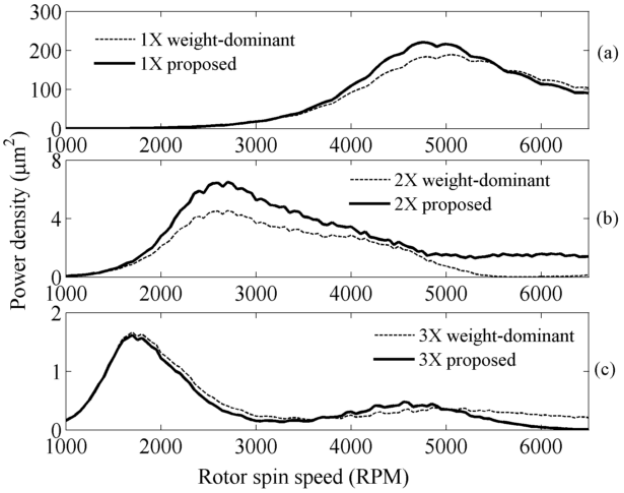

Figure 7. Change in (a) 1X, (b) 2X and (c) 3X harmonic components of the left bearing vertical vibration. $m_{ed} = 8\times10^{-5}$ kg·m and $\beta = 0°$.

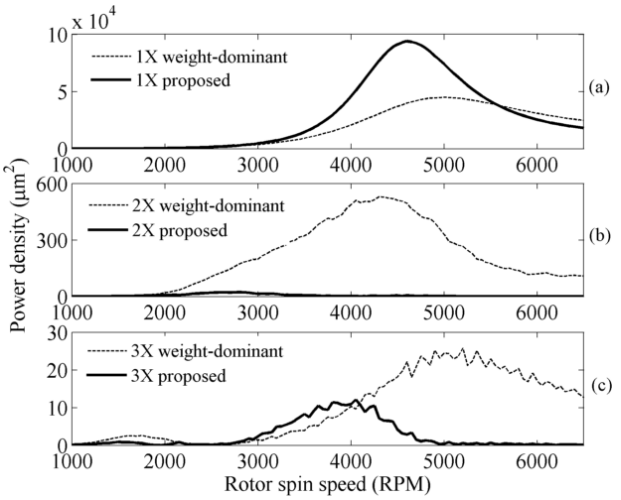

Figure 8. Change in (a) 1X, (b) 2X and (c) 3X harmonic components of the left bearing vertical vibration. $m_{ed} = 1\times10^{-3}$ kg·m and $\beta = 0°$.

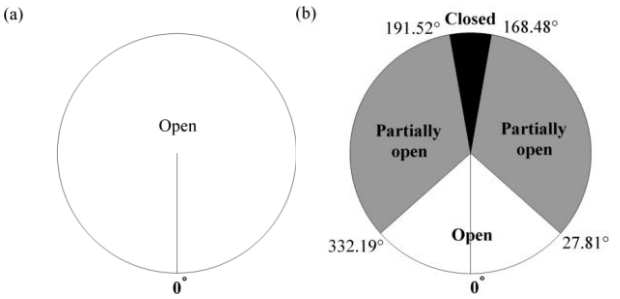

Figure 9. Predicted breathing behavior of (a) proposed model and (b) weight-dominant model at 4500 RPM.

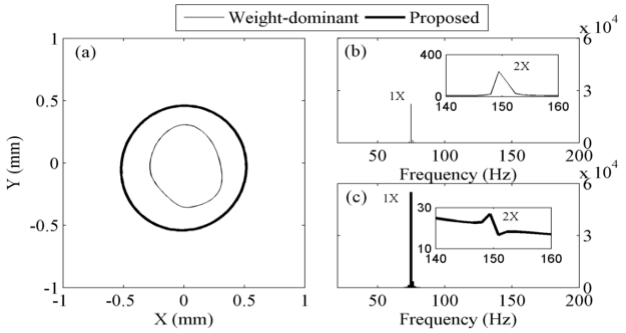

Figure 10. Trajectory and vertical power spectra of the left bearing at 4500 RPM (75 Hz) with eccentric mass placed at $\beta = 0°$ and $m_{ed} = 10^{-3}$.

V. Conclusion

This study examines a potential procedure for studying the vibration behavior of a cracked rotor with large permissible residual unbalance by removing the assumption of weight-dominance. Firstly, a new crack breathing mechanism suitable for predicting the vibration behavior of a cracked rotor with significant unbalance was formulated. The difference in vibration predicted through the proposed unbalance breathing model and the existing weight-dominant model was then examined.

The predicted vibration behavior of the two models was shown to have a high degree of similarity when the unbalance magnitude was relatively low (10^{-4} kg·m). However, when the unbalance magnitude was increased to 10^{-3} kg·m, the behaviors diverged. In particular, the proposed and weight-dominant models provided distinctly different predictions regarding the change in critical speed and peak amplitude response when gradually changing the location of the unbalance mass from 0 ° to 180 °. As the unbalance angle approached 180 °, the peak amplitude and critical speed response was shown to vary in an almost sinusoidal manner for the weight-dominant model. On the other hand, the peak amplitude response and critical speed for the proposed model varied in a non-sinusoidal manner and saw a plateau in values when the unbalance angle was close to 180 °.

Additionally, less emphasis on the sub-critical peaks (occurring at one-half and one-third of the critical speed) were seen as a result of increasing in unbalance magnitude due to the unbalance excitation force dominating the effects of the breathing mechanism.

Examination of the synchronous (1X) and supersynchronous (2X and 3X) vertical vibration components of the left bearing further supported that a reduction of unbalance causes the proposed and weight-dominant models to converge. For a larger unbalance magnitude (1×10^{-3} kg·m), a highly discernable difference in the change of the 2X component was predicted between the two models. The difference is suggested to be due to the weight-dominant model predicting the crack to continue breathing normally (gradual opening and closing of the crack), however the proposed model suggests the crack remains fully open. The crack remaining in a single state (always open) is known to be possible, particularly when the unbalance mass is large enough and placed at the same position as the crack ($\beta = 0°$).

The findings in this study make it clear that the discrepancy in breathing behavior of the proposed and weight-dominant models results in a significant difference in vibration behavior. As such, using a weight-dominant model for cracked rotors with large permissible residual unbalance becomes unsuitable for predicting vibration and for use in crack detection models.

Acknowledgment

We would like to thank Dr. Keqin Xiao for the continued support and the editing provided for this work.

References

[1] N. Bachschmid, P. Pennacchi, and E. Tanzi, *Cracked Rotors: A Survey on Static and Dynamic Behaviour Including Modelling and Diagnosis*, Springer Berlin Heidelberg, 2010.

[2] L. Cheng, N. Li, X. F. Chen, and Z. J. He, "The influence of crack breathing and imbalance orientation angle on the characteristics of the critical speed of a cracked rotor," *Journal of Sound and Vibration*, vol. 330, pp. 2031-2048, 2011.

[3] L. Rubio, B. Muñoz-Abella, P. Rubio, and L. Montero, "Quasi-static numerical study of the breathing mechanism of an elliptical crack in an unbalanced rotating shaft," *Latin American Journal of Solids & Structures*, vol. 11, pp. 2333-2350, 2014.

[4] A. K. Darpe, K. Gupta, and A. Chawla, "Transient response and breathing behaviour of a cracked Jeffcott rotor," *Journal of Sound and Vibration*, vol. 272, pp. 207-243, 2004.

[5] S. El Arem and Q. Nguyen, "Nonlinear dynamics of a rotating shaft with a breathing crack," *Annals of Solid and Structural Mechanics*, vol. 3, pp. 1-14, 2012.

[6] I. W. Mayes and W. G. R. Davies, "Analysis of the response of a multi-rotor-bearing system containing a transverse crack in a rotor," *Journal of Vibration, Acoustics, Stress, and Reliability in Design*, vol. 106, pp. 139-145, 1984.

[7] M. A. Al-Shudeifat, E. A. Butcher, and C. R. Stern, "General harmonic balance solution of a cracked rotor-bearing-disk system for harmonic and sub-harmonic analysis: Analytical and experimental approach," *International Journal of Engineering Science*, vol. 48, pp. 921-935, 2010.

[8] M. A. Al-Shudeifat and E. A. Butcher, "New breathing functions for the transverse breathing crack of the cracked rotor system: Approach for critical and subcritical harmonic analysis," *Journal of Sound and Vibration*, vol. 330, pp. 526-544, 2011.

[9] C. Guo, M. A. Al-Shudeifat, J. Yan, L. A. Bergman, D. M. McFarland, and E. A. Butcher, "Application of empirical mode decomposition to a Jeffcott rotor with a breathing crack," *Journal of Sound and Vibration*, vol. 332, pp. 3881-3892, 2013.

[10] R. D. Cook, *Concepts and applications of finite element analysis*, 4th Edition, New York: Wiley, 2002.

[11] Y. Ishida and T. Yamamoto, *Linear and Nonlinear Rotordynamics: A Modern Treatment with Applications*, Wiley, Hoboken, 2013.

Mr. Joseph Spagnol is a PhD student at the School of Computing, Engineering and Mathematics at Western Sydney University, Australia. He was awarded a Bachelor Degree in Mechanical Engineering, at WSU in 2015. His research has been focused on vibration analysis of a cracked rotor with an unbalance influenced breathing mechanism.

Dr. Helen Wu is a senior lecturer at the School of Computing, Engineering and Mathematics at Western Sydney University, Australia. Helen was awarded a Bachelor Degree in Mechanical Engineering at Sichuan University, China and a PhD in Civil Engineering at the University of Technology, Sydney. She has twenty years of experience in teaching, research and consulting relating to the dynamic response of materials, machines and structures including vibration and condition monitoring.

Associate Professor Chunhui Yang joined the School of Computing, Engineering and Mathematics at Western Sydney University, Australia in 2012. He was awarded a PhD in Mechanical Engineering at the University of Hong Kong in 2002. He has been working in computational mechanics focusing on characterization of material properties including multi-scale modeling of materials, structures, manufacturing and metal surface treatment. He has published more than 100 journal and conference papers.